

Geophysical Characterization of the Chilean Seismological Stations: First Results

by F. Leyton, A. Leopold, G. Hurtado, C. Pastén, S. Ruiz, G. Montalva, and E. Saéz

ABSTRACT

The Chilean Seismological Network has been rapidly growing in recent years, going from a few dozens stations working before 2010 to nearly a 100 installed all over the territory. Even more, nearly 300 strong-motion stations from the Accelerographic National Network have recently complemented this network, mainly deployed in large cities, at a variety of site conditions. All of these stations are currently providing useful information of Chilean earthquakes and are expected to record moderate-to-large events. However, the lack of appropriate site characterization sets an important limit to its usefulness. In this work, we present the geophysical characterization of 163 stations, the first results of larger effort to complete the characterization at all sites, based on array measurements of microtremors and horizontal-to-vertical spectral ratios. This information will help improve our understanding of the dynamic behavior of soils during earthquakes, providing relevant information for seismic design and seismic codes.

Electronic Supplement: Figures showing distribution of the geophones, and table with nearly 400 seismic stations managed by the Centro Sismológico Nacional of Universidad de Chile (CSN), along with their location and, the average S -wave velocity in the upper 30 m and the horizontal-to-vertical spectral ratio.

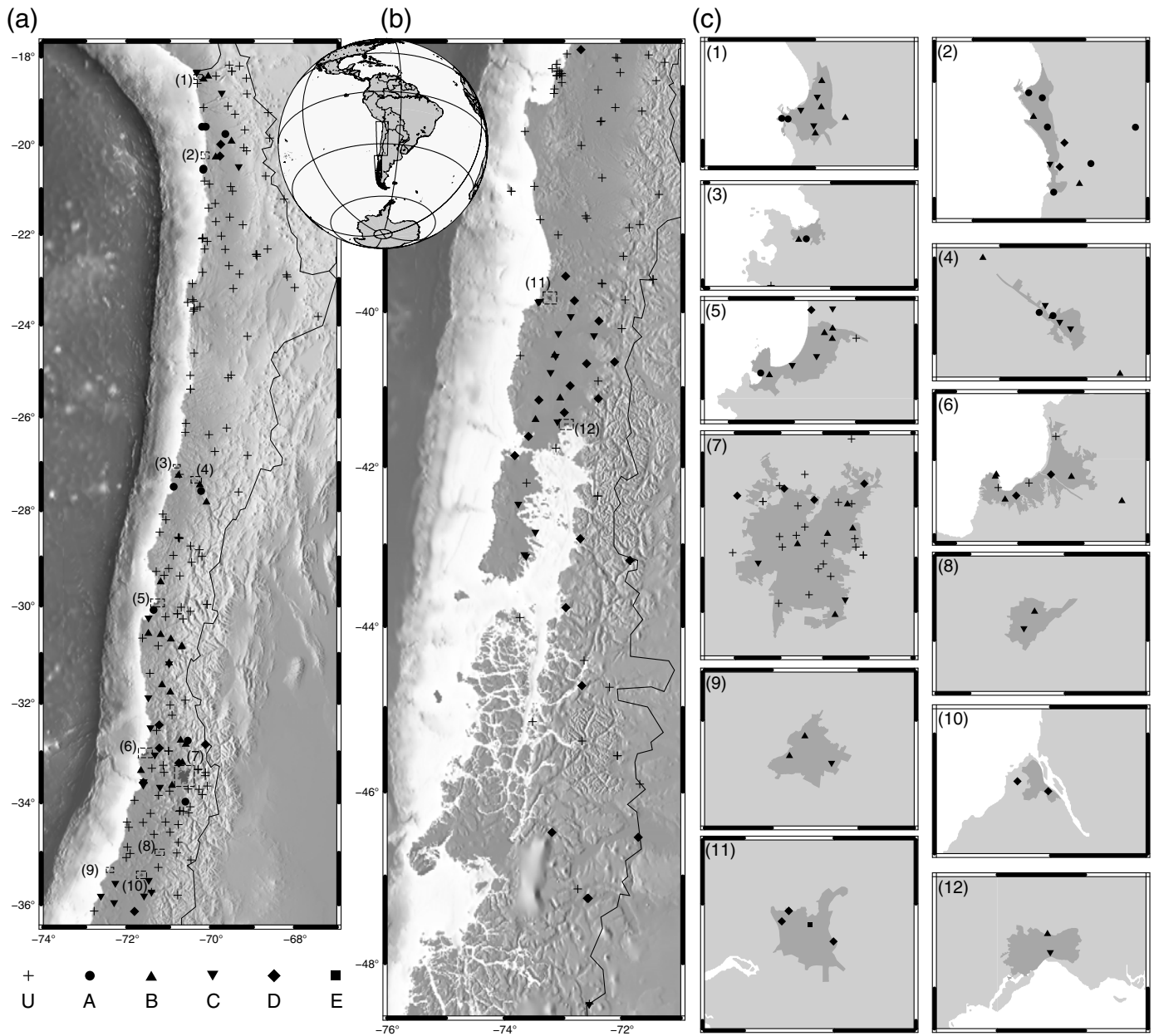
INTRODUCTION

The Chilean Seismological Network has been growing not only in number of stations but also in the type of instruments that they have. Since 2012, the National Seismological Center of the University of Chile (Centro Sismológico Nacional [CSN]) is operating more than 100 stations, composed of broadband seismometers, accelerometers, and Global Navigation Satellite Systems instruments, with their data being transmitted in real time to the analysis center (Barrientos, 2018; CSN, 2017; see [Data and Resources](#)). More recently, the National Office of Emergency and Mitigations has transferred

nearly 300 strong-motion stations (Red Nacional de Acelerómetros [RNA]) to the CSN, to be operated along with the rest of the network. These instruments from the RNA network are located throughout the whole country, concentrated in cities and other populated areas (see [Fig. 1](#)); this distribution gives a unique opportunity to improve our knowledge of the behavior of soil deposits during earthquakes, especially in urbanized areas. All the data collected by these networks are freely available and can be downloaded at any time (Chilean Strong-Motion Database, 2017; see [Data and Resources](#)). Moreover, the CSN is currently beginning a large effort to systematically characterize the local site conditions where all these stations are located.

It has clearly been established that local site conditions strongly modify the shaking produced by large earthquakes; moreover, it has been observed that damage produced by large earthquakes is strongly controlled by these conditions (Seed *et al.*, 1976). Currently, several seismic codes adopted a number of geophysical measurements for classification related to seismic site amplifications, being the harmonic or time-weighted average of the upper 30 m of the S -wave profile (V_{S30}) the most popular (Dobry *et al.*, 2000). Furthermore, recent studies suggest that V_{S30} , being useful in most cases, fails to capture the effect of thick sediments (Steidl, 2000; Régnier *et al.*, 2014) and might even overestimate the ground-motion amplitudes for a given frequency range (Park and Hashash, 2004), having the need to complement it with other sources of information such as the predominant site frequency (Cadet *et al.*, 2010).

Several methods have been used to determine the properties of the upper layers at a site, including invasive and non-invasive methods. These last ones are particularly preferred due to their lower costs and interesting capabilities of describing the subsurface structure (Aki, 1957; Asten and Henstridge, 1984; Horike, 1985). In the present study, we focus on array-based, surface-wave methods, shown to be able to perform correctly in Chile (Humire *et al.*, 2014; Kayen *et al.*, 2014; Molnar *et al.*, 2015). We complement these procedures with the well-known horizontal-to-vertical spectral ratio (HVSr), which has become increasingly popular (Pilz *et al.*, 2010; Molnar *et al.*,



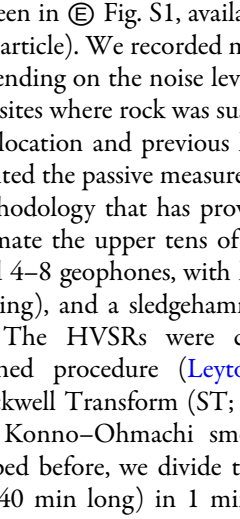
▲ **Figure 1.** Maps showing the stations belonging to the National Seismic Network managed by the Centro Sismológico Nacional: (a) northern Chile, from 17.7° S to 36.4° S, (b) southern Chile from 36.4° S to 48.6° S; each symbol represents a seismic station depending on the average S -wave velocity of the upper 30 m (V_{S30}), following the legend on the lower left. U represents those sites without a V_{S30} value, from A to E follow the classification shown in Table 1. The inset between (a) and (b) shows the studied region. (c) Zoom-in view for the following Chilean cities: (1) Arica, (2) Iquique, (3) Caldera, (4) Copiapó, (5) La Serena and Coquimbo, (6) Valparaíso and Viña del Mar, (7) Santiago, (8) Curicó, (9) Talca, (10) Constitución, (11) Valdivia, and (12) Puerto Montt.

2015) and has been successfully used to estimate the fundamental frequency of the site in Chile (Leyton *et al.*, 2013; Becerra *et al.*, 2015). In the present study, we use microtremor measurements to estimate the geophysical properties of the upper layers of 163 sites with strong-motion stations. We focus on the methodologies that enable us to investigate up to a significant depth and can be used in urban areas, with strong influence of anthropogenic seismic noise.

METHODOLOGY

In this study, we used mostly passive surface-wave methods to extract dispersion curves via spatial autocorrelation (Aki, 1957; Asten and Henstridge, 1984) or frequency–wavenumber (Horike, 1985); complemented with the single-station measurements of the HVSr. For all the measurements, we used three-component seismographs, with reliable frequency range

from 0.1 to 1024 Hz (Tromino, 2017; see [Data and Resources](#)); these instruments have previously shown their suitability for these kinds of studies ([Humire et al., 2014](#); [Becerra et al., 2015](#); [Molnar et al., 2015](#)). In the present work, we only used the vertical components for the array processing, whereas the horizontal ones were considered to compute the HVSR.

The field procedure was explained in detail in a previous work ([Leyton et al., 2017](#)); nevertheless, in a few words, we deploy instruments in the area around the station in two arrays: a large irregular quadrilateral, covering the largest possible distances, and an equilateral triangle with a central station, covering distances ranging from 10 to 30 m (an example can be seen in  Fig. S1, available in the electronic supplement to this article). We recorded microtremors from 20 up to 40 min, depending on the noise level at the time of the measurements. For sites where rock was suspected to be near the surface, given the location and previous knowledge of the area, we complemented the passive measurements using active source methods, methodology that has proven to give enough information to estimate the upper tens of meters ([Humire et al., 2014](#)). We used 4–8 geophones, with linear arrays configurations (4–7 m spacing), and a sledgehammer as active source.

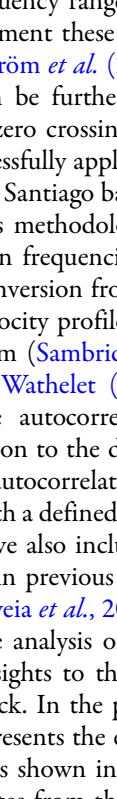
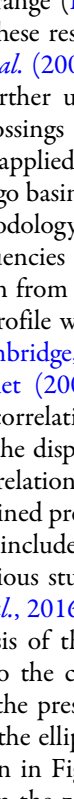
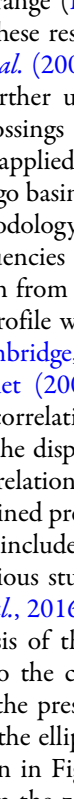
The HVSRs were computed following a previously defined procedure ([Leyton et al., 2012](#)), based on the Stockwell Transform (ST; [Stockwell et al., 1996](#)), rather than the Konno–Ohmachi smoothed Fourier spectrum. As described before, we divide the complete time window (usually 20–40 min long) in 1 min subwindows, each one processed in the same way. We obtain the ST of each trace and compute the total horizontal energy by adding the amplitude of both horizontal components, without including the phase. Next, for each time step, we compute the HVSR for a frequency range from 0.1 to 10 Hz; the final HVSR curve is the overall average of all subwindows. Given the fact that the ST considers nearby values for each frequency, we cannot use the standard deviation as an estimation of the error for each point. Therefore, we estimate it by considering the value where 68.2% of the observations from all subwindows are considered; some examples are shown in [Figure 2](#). To simplify the interpretation of the HVSR results, we relate the peak amplitude to an amplitude classification ($HVSR_{amp}$), as proposed by [Idini et al. \(2017\)](#) and shown in [Figure 2](#). In this figure, we present the amplitude classification of $HVSR_{amp}$: curves with HVSR amplitude lower than 2 (flat curve) classified as $HVSR_{amp} = 0$, curves with HVSR amplitude from 2 to 3 correspond to $HVSR_{amp} = 1$, curves with HVSR amplitude from 3 to 5 are classified with $HVSR_{amp} = 2$, and curves with HVSR amplitude from 5 and above with $HVSR_{amp} = 3$. For those curves with $HVSR_{amp} \geq 1$ (HVSR peak amplitude larger than 2), the predominant frequency is defined as the corresponding frequency at the peak. Estimations of the predominant frequency from strong-motion records, as done in [Zhao et al. \(2006\)](#) are presented in a companion paper ([Leyton et al., 2017](#)).

In the present study, we mostly used the SPatial AutoCorrelation (SPAC) methodology, first proposed by [Aki \(1957\)](#)

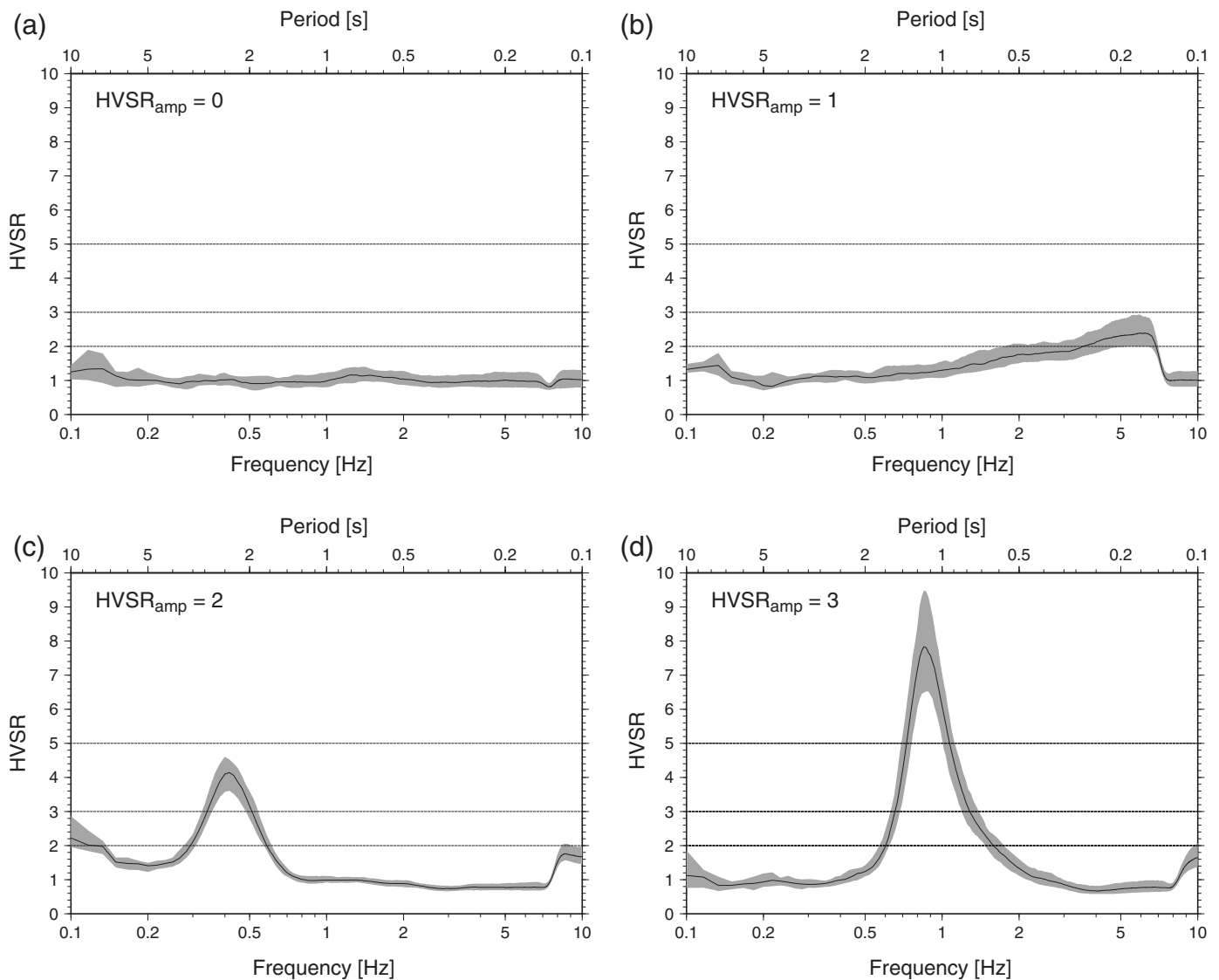
and later modified for more general configurations by [Chávez-García et al. \(2005, 2006\)](#). This methodology has shown to be able to explore the characteristics of the dispersion curves in the lower frequency range ([Humire et al., 2014](#)). Furthermore, we complement these results with the method recently proposed by [Ekström et al. \(2009\)](#), who noticed that the same methodology can be further used to higher frequencies, by focusing on the zero crossings ([Ekström, 2014](#)). [Pastén et al. \(2016\)](#) have successfully applied these techniques to determine deep layers of the Santiago basin; in the present study, we were able to apply this methodology to characterize the shallower layers, focusing on frequencies from 10 Hz and above.

Finally, the inversion from the obtained dispersion curves to the *S*-wave velocity profile was performed using the neighborhood algorithm ([Sambridge, 1999](#)), appropriately adapted for this case by [Wathelet \(2005, 2008\)](#). For the inversion, we included the autocorrelation results, from the SPAC method, in addition to the dispersion estimates from the zero crossings of the autocorrelation ratios ([Ekström et al., 2009](#)). For those sites with a defined predominant frequency (i.e., with $HVSR_{amp} \geq 1$), we also included the average curve in the inversion, as done in previous studies ([Picozzi et al., 2005](#); [Pilz et al., 2010](#); [Gouveia et al., 2016](#)). The inclusion of the HVSR curve enables the analysis of the deeper parts of the profile, usually giving insights to the contrast between soils and the underlying bedrock. In the present study, we assume that the HVSR curve represents the ellipticity of the Rayleigh wave. A general example is shown in [Figure 3](#), using dispersion curve, dispersion estimates from the zero crossings of the autocorrelation ratios, and HVSR for the inversion. From this example, we can see that the shallow part of the profile is determined from the dispersion curve, considering frequencies above 4 Hz. On the other hand, the deeper parts of the profile are mainly constrained by the ellipticity curve, including the lower end of frequencies, below 4 Hz for this case.

RESULTS

We were able to successfully obtain 163 *S*-wave velocity profiles and predominant frequencies for seismological stations' sites of the Chilean Seismic Network, as shown in [Figure 1](#) and  Table S1. A histogram of the latitudinal distribution of the sites' classification is presented in  Figure S2. From this  Figure S2, we see that even though we still need to measure a considerable number of stations, the northern Chile (north of $\sim 35^\circ\text{S}$) is characterized to have $V_{S30} \geq 350$ m/s (class C and above, according to the V_{S30} classification shown in [Table 1](#)). On the other hand, south of 39°S , most of the stations are characterized to have $V_{S30} \leq 500$ m/s, mostly classes C and D, with few E from the V_{S30} classification presented in [Table 1](#). These preliminary observations need to be revised upon the completion of the site characterization of the whole network.

To improve our understanding of the results, we plotted V_{S30} as a function of the predominant frequency for each site (see [Fig. 4](#)); the $HVSR_{amp}$ is shown as the size of the cross (see [Fig. 4](#) caption for details). In [Figure 4](#), the black squares mark

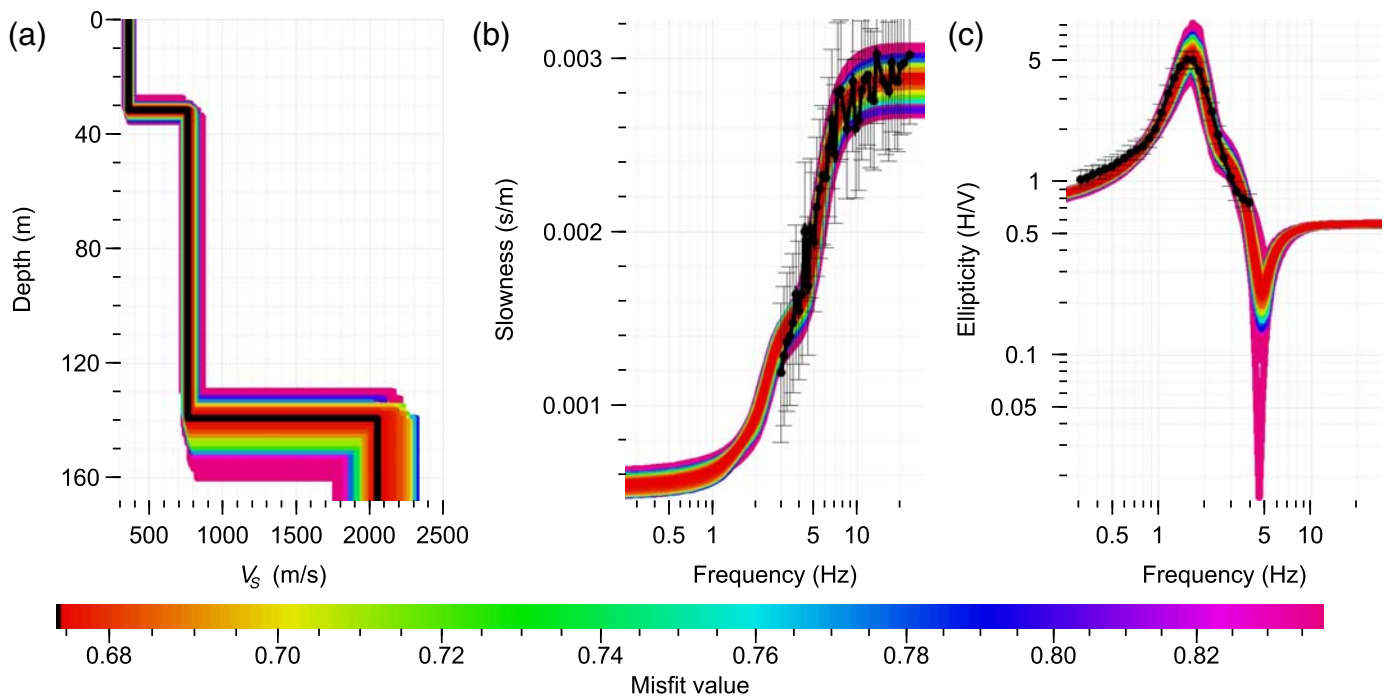


▲ **Figure 2.** Examples of horizontal-to-vertical spectral ratio (HVSr) of microtremors; continuous line shows the geometric average for each subwindows and the gray area represents the error (see the [Methodology](#) section for details). Each panel shows a different amplitude classification ($HVSr_{amp}$), falling between the limits shown in thin lines: (a) flat curve ($HVSr_{amp} = 0$), (b) small amplitude ($HVSr_{amp} = 1$), (c) medium amplitude ($HVSr_{amp} = 2$), and (d) large amplitude ($HVSr_{amp} = 3$).

the average predominant frequency for classes B, C, and D. We expect to have an inverse correlation between V_{S30} and the $HVSr_{amp}$: sites with soft soils (lower V_{S30} values) should have a larger impedance contrast with the basement rock, producing larger $HVSr_{amp}$. On the other hand, the predominant frequency depends not only on the S -wave velocity values but also on the soil's thickness; hence, no clear correlation should be found due to the lack of information of this last parameter. From Figure 4, we can see that there is no clear correlation between V_{S30} and the predominant period, as has been proposed in some seismic design codes (e.g., [Japan Road Association, 1980, 1990](#)); nevertheless, it might be suggested that for sites with $V_{S30} \leq 500$ m/s, they mostly show predominant frequencies lower than 3 Hz (marked with a dashed line in Fig. 4). Furthermore, we computed the Spearman correlation

coefficient (r_s) between V_{S30} , predominant frequency, and $HVSr_{amp}$. We found almost no correlation between the predominant frequency and the $HVSr_{amp}$ ($r_s = 0.0785$), as suspected. On the other hand, we obtained a slightly higher correlation between the V_{S30} and the $HVSr_{amp}$, but still very low ($r_s = 0.3399$); this might be due to the fact that V_{S30} is not always a good estimator of the average S -wave velocities in the soils and the implied impedance contrast with the bedrock. Finally, the best correlation was found between the V_{S30} and the predominant frequency, with a value of $r_s = 0.5494$, despite the limitations of V_{S30} as an indicator of the average S -wave velocities in the soils and the need to specify the soil's thickness.

For our data set, out of the 163 sites studied, 40 of them presented no clear predominant frequency from 0.1 to 10 Hz

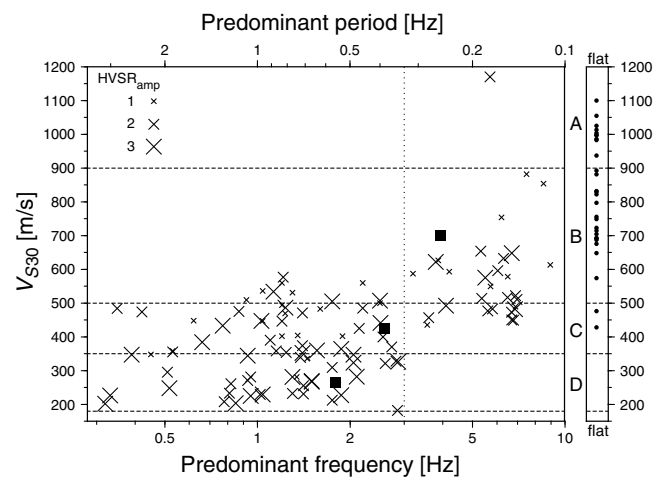


▲ **Figure 3.** Example of *S*-wave profile inversion, where we considered the dispersion curve and ellipticity; all panels present the misfit of different models, following the same color palette shown in the bottom. (a) *S*-wave velocity as a function of depth, black line shows the best fit. For (b,c), the thin black lines and dots show the values obtained from the microtremors measurements, whereas the individual lines are the fir for different models, following the scale shown in the bottom. (b) The dispersion curve; (c) the ellipticity. The color version of this figure is available only in the electronic edition.

(flat curves), shown in the right panel in Figure 4, representing a 25% of the total. For these sites, 94% of them have V_{S30} above 640 m/s; only three cases present V_{S30} values lower, indicating that flat curves do not necessarily imply high V_{S30} .

FINAL COMMENTS

In this study, we report preliminary results of the geophysical characterization of the Chilean Seismological Network, managed by CSN, mostly using active- and passive-source surface-wave array methods, and the HVSr method. The geophysical characterization using these methods was particularly difficult due to the fact that most of these stations are located in mod-



▲ **Figure 4.** Average *S*-wave velocity in the upper 30 m (V_{S30}) as a function of the predominant frequency (bottom scale) or period (upper scale) for the all the site studied here. The size of each cross is proportional to the amplitude classification ($HVSR_{amp}$), following the legend in the upper left corner. The black squares shows the average predominant frequency for classes B, C, and D. Thin black lines mark the classification used in this study, also presented in Table 1; the vertical dotted line marks the 3 Hz predominant frequency. The right panel shows the V_{S30} for sites with flat curves (e.g., $HVSR_{amp} = 0$).

Classification	V_{S30} Range (m/s)
A	$900 \leq V_{S30}$
B	$500 \leq V_{S30} \leq 900$
C	$350 \leq V_{S30} \leq 500$
D	$180 \leq V_{S30} \leq 350$
E	$V_{S30} \leq 180$

erate-to-large cities, with high urban noise. We successfully explore 163 stations, using array-based and three-component microtremor measurements. The most reliable methods used in the present study were SPAC (Aki, 1957) and its extension to higher frequency considering only the zero crossings (Ekström *et al.*, 2009; Ekström, 2014). We found that there is no clear correlation between the site's predominant frequency and the HVSR amplitude (HVSR_{amp}); however, there seems to be a slight correlation between the average *S*-wave velocity in the upper 30 m (V_{S30}) and the predominant frequency: from our results, sites with $V_{S30} \leq 500$ m/s appear to have a predominant frequency lower than 3 Hz. We believe that this information will contribute to the understanding of the strong-motion shaking produced by large-to-moderate earthquakes, especially in sites where most of the Chilean population live.

DATA AND RESOURCES

The authors, using instruments from the Department of Geophysics of University of Chile, and Departments of Civil Engineering from P. Catholic University of Chile and University of Concepción, collected the data used in this study. The information on Chilean Strong-Motion Database (2017) can be found at evtdb.csn.uchile.cl, which is managed by National Seismological Center. The data on Centro Sismológico Nacional (CSN) (2017) are available at www.csn.uchile.cl (Universidad de Chile). The other data are from www.tromino.eu (Tromino, from Moho, Science and Technology). ☒

ACKNOWLEDGMENTS

The authors would like to thank the Geopsy Team for making freely available its software for the processing of microtremors (Wathelet, 2002–2011). The authors thank S. Molnar, an anonymous reviewer, and Editor-in-Chief Zhigang Peng for their valuable comments that greatly improved this article. The article also would like to thank C. Benitez, S. Droguett, L. Podestá, and P. Troncoso for their help during the Tarapacá campaign and J. Salomón for his help during the Coquimbo campaign. Figures were made using Generic Mapping Tools (GMT) software (Wessel and Smith, 1998). The authors acknowledge the support of the National Fund for Scientific and Technological Research (FONDECYT) Project No. 1170430.

REFERENCES

Aki, K. (1957). Space and time spectra of stationary stochastic waves, with special reference to microtremors, *Bull. Earthq. Res. Inst.* **35**, 415–457.
 Asten, M. W., and J. D. Henstridge (1984). Array estimators and use of microseisms for reconnaissance of sedimentary basins, *Geophysics* **49**, 1828–1837.
 Barrientos, S. (2018). The new Chilean seismic network, *Seismol. Res. Lett.* doi: [10.1785/0220160195](https://doi.org/10.1785/0220160195).
 Becerra, A., L. Podestá, R. Monetta, E. Sáez, F. Leyton, and G. Yañez (2015). Seismic microzoning of Arica and Iquique, Chile, *Nat. Hazards* **79**, no. 1, 567–586, doi: [10.1007/s11069-015-1863-y](https://doi.org/10.1007/s11069-015-1863-y).

Cadet, H., P. Y. Bard, and A. Rodríguez-Marek (2010). Defining a standard rock site: Propositions based on the KiK-net database, *Bull. Seismol. Soc. Am.* **100**, 172–195.
 Chávez-García, F., M. Rodríguez, and W. Stephenson (2005). An alternative approach to the SPAC analysis of microtremors: Exploiting stationarity of noise, *Bull. Seismol. Soc. Am.* **95**, 277–293.
 Chávez-García, F., M. Rodríguez, and W. Stephenson (2006). Subsoil structure using SPAC measurements along a line, *Bull. Seismol. Soc. Am.* **96**, 729–736.
 Dobry, R., R. D. Borcherdt, C. B. Crouse, I. M. Idriss, W. B. Joyner, G. R. Martin, M. S. Power, E. E. Rinne, and R. B. Seed (2000). New site coefficients and site classification system used in recent building seismic code provisions, *Earthq. Spectra* **16**, no. 1, 41–67.
 Ekström, G. (2014). Love and Rayleigh phase-velocity maps, 5–40 s, of the Western and Central USA from USArray data, *Earth Planet. Sci. Lett.* **402**, 42–49.
 Ekström, G., G. A. Abers, and S. C. Webb (2009). Determination of surface-wave phase velocities across USArray from noise and Aki's spectral formulation, *Geophys. Res. Lett.* **36**, no. 18, 5–9.
 Gouveia, F., I. Lopes, and R. C. Gomes (2016). Deeper V_S profile from joint analysis of Rayleigh wave data, *Eng. Geol.* **202**, 85–98.
 Horike, M. (1985). Inversion of phase velocity of long-period microtremors to the *S*-wave-velocity structure down to the basement in urbanized areas, *J. Phys. Earth* **33**, 59–96.
 Humire, F., E. Sáez, F. Leyton, and G. Yañez (2014). Combining active and passive multi-channel analysis of surface waves to improve reliability of $V_{S,30}$ estimation using standard equipment, *Bull. Earthq. Eng.* **13**, no. 5, 1303–1321, doi: [10.1007/s10518-014-9662-5](https://doi.org/10.1007/s10518-014-9662-5).
 Idini, B., F. Rojas, S. Ruiz, and C. Pastén (2017). Ground motion prediction equations for the Chilean subduction zone, *Bull. Earthq. Eng.* **15**, no. 5, 1853–1880, doi: [10.1007/s10518-016-0050-1](https://doi.org/10.1007/s10518-016-0050-1).
 Instituto Nacional de Normalización (2012). *Earthquake Resistant Design of Buildings*, NCh433of1996mod2012, Instituto Nacional de Normalización, Chile.
 Japan Road Association (1980). *Specifications for highway bridges: Part V. Seismic Design*, Maruzen Co., LTD, Tokyo, Japan.
 Japan Road Association (1990). *Specifications for highway bridges: Part V. Seismic Design*, Maruzen Co., LTD, Tokyo, Japan.
 Kayen, R., B. D. Carkin, S. Corbet, C. Pinilla, A. Ng, E. Gorbis, and C. Truong (2014). Seismic velocity site characterization of thirty-one Chilean seismometer stations by spectral analysis of surface wave dispersion, *Technical Report PEER 2014/05*, Pacific Earthquake Engineering Research, Berkeley, California.
 Leyton, F., C. Pastén, S. Ruiz, B. Idini, and F. Rojas (2017). Empirical site classification of CSN network using strong-motion records, *Seismol. Res. Lett.* doi: [10.1785/0220170167](https://doi.org/10.1785/0220170167).
 Leyton, F., S. Ruiz, and M. Astroza (2012). Correlation between seismic intensity for the Maule 2010 earthquake (M_w 8.8) and microtremors' HVSR, *15th World Conf. on Earthquake Engineering*, Lisboa, Portugal, 24–28 September, 2012, Paper Number 1428.
 Leyton, F., S. Ruiz, S. A. Sepúlveda, J. P. Contreras, S. Rebolledo, and M. Astroza (2013). Microtremors' HVSR and its correlation with surface geology and damage observed after the 2010 Maule earthquake (M_w 8.8) at Talca and Curicó, Central Chile, *Eng. Geol.* **161**, 26–33, doi: [10.1016/j.enggeo.2013.04.009](https://doi.org/10.1016/j.enggeo.2013.04.009).
 Molnar, S., C. E. Ventura, R. Boroschek, and M. Archila (2015). Site characterization at Chilean strong-motion stations: Comparison of downhole and microtremor shear-wave velocity methods, *Soil Dynam. Earthq. Eng.* **79**, no. 2015, 22–35.
 Park, D., and Y. M. A. Hashash (2004). Probabilistic seismic hazard analysis with nonlinear site effects in the Mississippi embayment, *Proc. 13th World Conf. Earthq. Eng.*, Vancouver, British Columbia, 1–6 August, CD-Rom Edition, Paper Number 1549.
 Pastén, C., M. Sáez, S. Ruiz, F. Leyton, J. Salomón, and P. Poli (2016). Deep characterization of the Santiago basin using HVSR and cross-correlation of ambient seismic noise, *Eng. Geol.* **201**, 57–66.

- Picozzi, M., S. Parolai, and S. M. Richwalski (2005). Joint inversion of H/V ratios and dispersion curves from seismic noise: Estimating the S-wave velocity of bedrock, *Geophys. Res. Lett.* **32**, L11308, doi: [10.1029/2005GL022878](https://doi.org/10.1029/2005GL022878).
- Pilz, M., S. Parolai, M. Picozzi, R. Wang, F. Leyton, J. Campos, and J. Zschau (2010). Shear wave velocity model of the Santiago de Chile basin derived from ambient noise measurements: A comparison of proxies for seismic site conditions and amplification, *Geophys. J. Int.* **182**, 355–367, doi: [10.1111/j.1365-246X.2010.04613.x](https://doi.org/10.1111/j.1365-246X.2010.04613.x).
- Régnier, J., L. F. Bonilla, E. Bertrand, and J.-F. Semblat (2014). Influence of the Vs profiles beyond 30 m depth on linear site effects: Assessment from the KiK-net data, *Bull. Seismol. Soc. Am.* **104**, 2337–2348.
- Sambridge, M. (1999). Geophysical inversion with a neighborhood algorithm: I. Searching a parameter space, *Geophys. J. Int.* **138**, 479–494.
- Seed, H. B., C. Ugas, and J. Lysmer (1976). Site-dependent spectra for earthquake-resistant design, *Bull. Seismol. Soc. Am.* **66**, 221–243.
- Steidl, J. H. (2000). Site response in Southern California for probabilistic seismic hazard analysis, *Bull. Seismol. Soc. Am.* **90**, 149–169.
- Stockwell, R. G., L. Mansinha, and R. P. Lowe (1996). Localization of the complex spectrum: The S transform, *IEEE Trans. Signal Process.* **44**, 998–1001.
- Wathelet, M. (2002–2011). *GEOPSY packages (Version 2.5.0)*, software, available at <http://www.geopsy.org/download.php>.
- Wathelet, M. (2005) *Array Recordings of Ambient Vibrations: Surface-Wave Inversion*, Liege University, Liege, Belgium.
- Wathelet, M. (2008). An improved neighborhood algorithm: Parameter conditions and dynamic scaling, *Geophys. Res. Lett.* **35**, no. 9, doi: [10.1029/2008GL033256](https://doi.org/10.1029/2008GL033256).
- Wessel, P., and W. H. F. Smith (1998). New improved version of generic mapping tools released, *Eos Trans. AGU* **79**, 579.
- Zhao, J. X., J. Zhang, A. Asano, Y. Ohno, T. Oouchi, T. Takahashi, H. Ogawa, K. Irikura, H. K. Thio, P. G. Somerville, *et al.* (2006). Attenuation relations of strong ground motion in Japan using site classification based on predominant period, *Bull. Seismol. Soc. Am.* **96**, 898–913.

F. Leyton
A. Leopold
G. Hurtado
Centro Sismológico Nacional

Universidad de Chile
Blanco Encalada 2002
Santiago, Chile
leyton@csn.uchile.cl
aleopold@csn.uchile.cl
ghurtado@csn.uchile.cl

C. Pastén
Department of Civil Engineering
Universidad de Chile
Blanco Encalada 2002
Santiago, Chile
cpasten@ing.uchile.cl

S. Ruiz
Department of Geophysics
Universidad de Chile
Blanco Encalada 2002
Santiago, Chile
sruiz@dgf.uchile.cl

G. Montalva
Department of Civil Engineering
Universidad de Concepción
Casilla 160-C, Correo 3
Concepción, Chile
gmontalva@udec.cl

E. Saéz
Department of Structural and Geotechnical Engineering
La Pontificia Universidad Católica de Chile
Av. Vicuña Mackenna 4860
Macul, Chile
esaez@ing.puc.cl

Published Online 7 February 2018